JTE
HCMUTE ISSN: 2615-9740

JOURNAL OF TECHNICAL EDUCATION SCIENCE
Ho Chi Minh City University of Technology and Education
Website: https://jte.edu.vn
Email: jte@hcmute.edu.vn

Static Analysis of the Honeycomb Sandwich Plate With GNPs Facesheets Using an Isogeometric Approach

Minh Anh Hoang, Tri Dung Nguyen, Tan Hung Pham*
Ho Chi Minh City University of Technology and Education, Vietnam

*Corresponding author. *Email: hungpht@hcmute.edu.vn*

ARTICLE INFO

Received: 12/06/2025
Revised: 17/09/2025
Accepted: 08/10/2025
Published: 28/11/2025

KEYWORDS

Static analysis;
Isogeometric analysis;
Refined plate theory;
Elastic foundation;
Auxetic honeycomb;
Graphene nanoplatelets.

ABSTRACT

This paper investigates the static behavior of auxetic honeycomb sandwich plates with graphene nanoplatelet (GNP)-reinforced aluminum face sheets based on a refined plate theory (RPT) and isogeometric analysis (IGA). The RPT incorporates the effects of transverse shear deformation without requiring shear correction factors, while the auxetic honeycomb core enhances the mechanical performance of the sandwich structure. The effective properties of the GNPs-reinforced composite face sheets are determined using a modified Halpin-Tsai micromechanical model under uniform nanoparticle distribution. Integrating RPT with IGA enables exact geometry representation and high-order continuity, offering advantages over conventional finite element method despite the higher computational cost for large basis functions. Numerical studies are carried out to evaluate the influence of parameters, such as nanoparticle weight fraction, honeycomb geometry, and boundary conditions on the static response of the sandwich plate. The results confirm the effectiveness and reliability of the proposed approach, highlighting that the combination of auxetic cores and GNPs reinforcement substantially improves structural stiffness and static behavior, providing useful guidance for the design of advanced lightweight structures.

Doi: https://doi.org/10.54644/jte.2025.1948

1. Introduction

The auxetic honeycomb sandwich structure is a lightweight material featuring a negative Poisson's ratio core between two face sheets, offering a superior strength-to-weight ratio for aerospace, automotive, and structural uses. Auxetic honeycombs offer superior shear stiffness, improved toughness, and greater indentation resistance compared to conventional cores. Recently, extensive research has explored their mechanical behavior through various theoretical and numerical approaches. Liu et al. [1] introduced a semi-analytical approach for evaluating the bending, buckling, and vibration behaviors of sandwich panels with square-honeycomb cores. [2] employed a novel theoretical model to investigate the buckling of hexagonal honeycomb sandwich panels using the finite element method (FEM). The buckling analysis of the sandwich shells with honeycomb core using the first order-shear deformation theory (FSDT) and analytical method was performed by Thang [3]. Based on the fourth-order shear deformation theory, Shirdelan et al. [4] studied the control and vibration of the doubly curved composite microshells with honeycomb core and piezoelectric layers. Singh et al. [5] found the vibrational frequency and buckling load of the auxetic honeycomb sandwich plate with the face layers made of functionally graded material (FGM). Yuan et al. [6] utilized the combination of FSDT and FEM to express the influence of the thermal on the vibration and buckling of the sandwich plate with multi-arc concave honeycomb core.

Graphene nanoplatelets (GNPs) have emerged as one of the most promising nanofillers for polymer matrix composites, attributed to their outstanding mechanical, thermal, and electrical properties. GNPs possess a high aspect ratio, excellent stiffness, and exceptional strength, making them ideal candidates for reinforcing lightweight composites in structural applications. Numerous investigations about the

structures reinforced by GNPs were performed using various methods by the researchers recently. Ebrahimi et al. [7] studied the size-dependent force vibration and buckling responses of the cylindrical nanoshells reinforced by GNPs using the analytical approach. Based on the higher-order shear deformation theory (HSDT) and Galerkin method, Khalaf et al. [8] introduced the nonlinear vibration of toroidal shells reinforced by carbon nanotubes (CNTs) and GNPs. In the study [9], Zhao et al. used FSDT and FEM to study the natural frequency behavior of functionally graded multilayer cylindrical shell panels reinforced with a hybrid combination of graphene nanoplatelets (GPLs) and CNTs. The thermal buckling and vibration behaviors of GNPs reinforced composite cylindrical nanoshells under bi-directional thermal loads using a modified couple stress theory (MCST) were performed by Li et al. [10].

Isogeometric analysis (IGA), originally introduced by Hughes et al. [11], represents a significant advancement in computational mechanics by seamlessly integrating computer-aided design (CAD) and finite element analysis (FEA). The nonlocal theory, HSDT and IGA were utilized by Nguyen et al. [12] to present the static and bending of the FG magneto-electro-elastic beams. Phung-Van et al. [13] used Eringen's nonlocal elasticity theory, HSDT and IGA to investigate the vibration and static analyses of the FG nanoplates. A refined sinus shear deformation theory and IGA were employed by Lezgy et al. [14] to find the frequency and deflection of the laminated composite beams. Considering the surface effect, Shi et al. [15] studied buckling, bending and vibration of the FG microplates based on TSDT, MCST and IGA. Although these studies confirm the accuracy and versatility of IGA for complex structures, most focus on conventional or FG plates and beams. To date, no work has addressed the static analysis of auxetic sandwich plates with GNP-reinforced face sheets using RPT and IGA. The novelty of the present study lies in combining RPT, which avoids shear correction factors, with IGA, which ensures exact geometry representation and efficient high-order approximation. This approach offers clear advantages over traditional FEM for modeling curved auxetic geometries, while acknowledging its higher computational cost for large basis functions. To fill this gap, the present research integrates RPT and IGA to examine the static bending characteristics of these advanced sandwich structures. The effects of geometrical characteristics of the auxetic core, and GNPs reinforcement on the deflection of the sandwich plate are thoroughly examined and discussed.

2. The basic equations

2.1. The governing equation

Consider a sandwich plate featuring an auxetic core and GNP face sheets, as illustrated in Figure 1. In this configuration, a, b, and h represent the length, width, and total thickness of the plate, respectively, while h_c and h_f denote the core and facesheets thickness, respectively. Additionally, l, t, d and θ correspond to the inclined length, thickness, horizontal length, and the inclined angle of the auxetic unit cell, respectively.

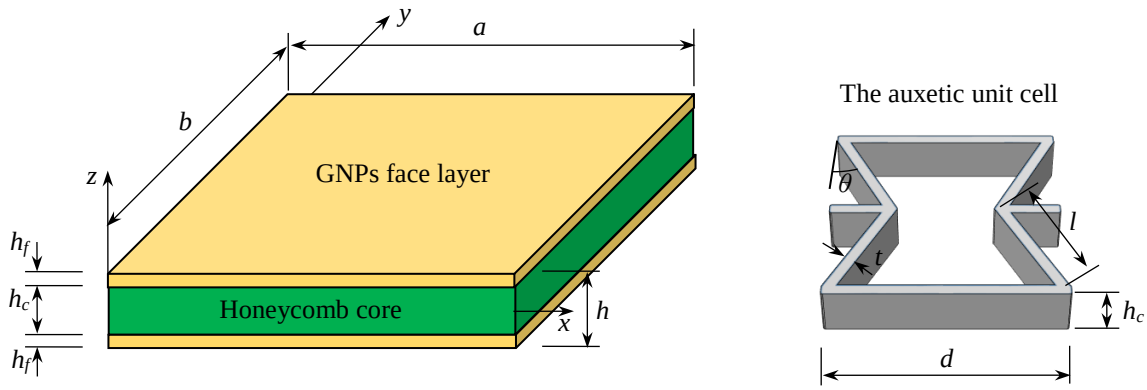

Figure 1. *The auxetic honeycomb sandwich plate with GNPs face layers.*

The face layers of the sandwich plate are made of an aluminum matrix strengthened with uniformly distributed GNPs. According to the Halpin-Tsai micromechanics model [16, 17], the effective Young's modulus of the face sheets is calculated by following

$$E_f = \frac{E_m}{8}\left(3\frac{1+\zeta_L\eta_L V_G}{1-\eta_L V_G}+5\frac{1+\zeta_W\eta_W V_G}{1-\eta_W V_G}\right) \tag{1}$$

in which

$$\zeta_L = \frac{2l_G}{t_G};\ \zeta_W = \frac{2w_G}{t_G};\eta_L = \frac{E_G-E_m}{E_G+E_m\zeta_L};\eta_W = \frac{E_G-E_m}{E_G+E_m\zeta_W} \tag{2}$$

where E_G and E_m represent the elastic moduli of GNPs and the matrix, respectively; l_G, w_G and t_G denote the GNPs length, width and thickness. The equivalent mass density (ρ) and Poisson's ratio (ν) are evaluated based on the rule of mixtures through the following relations

$$\begin{aligned}\rho_f &= \rho_m\left(1-V_G\right)+\rho_G V_G\\ \nu_f &= \nu_m\left(1-V_G\right)+\nu_G V_G\\ V_G &= \frac{W_G\rho_m}{W_G\rho_m+\rho_G\left(1-W_G\right)}\end{aligned} \tag{3}$$

in which symbols "*m*" and "*G*" indicate matrix and GNPs, respectively; V_G represents the volume fraction of GNPs; W_G is the GNPs volume fraction.

The effective material properties of the auxetic honeycomb core with a negative Poisson's ratio can be determined as follows [18, 19].

$$\begin{aligned}&E_{1c} = \frac{\eta_3^3\left(\eta_1-\sin\theta\right)E_h}{\cos^3\theta\left[1+\eta_3^2\left(\tan^2\theta+\eta_1\sec^2\theta\right)\right]}\ ;\ E_{2c} = \frac{\eta_3^3 E_h}{\left(\eta_1-\sin\theta\right)\left(\tan^2\theta+\eta_3^2\right)\cos\theta}\\ &G_{12c} = \frac{\eta_3^3 E_h}{\eta_1\cos\theta\left(1+2\eta_1\right)};G_{13c} = \frac{\eta_3 G_h}{2\cos\theta}\left[\frac{\eta_1-\sin\theta}{1+2\eta_1}+\frac{\eta_1+2\sin^2\theta}{2\left(\eta_1-\sin\theta\right)}\right];G_{23c} = \frac{\eta_3\cos\theta G_h}{\eta_1-\sin\theta}\\ &\nu_{12c} = \frac{-\sin\theta\left(1-\eta_3^2\right)\left(\eta_1-\sin\theta\right)}{\cos^2\theta\left[1+\eta_3^2\left(\tan^2\theta+\eta_1\sec^2\theta\right)\right]};\nu_{21c} = \frac{-\sin\theta\left(1-\eta_3^2\right)}{\left(\eta_1-\sin\theta\right)\left(\tan^2\theta+\eta_3^2\right)}\\ &\rho_c = \frac{\rho_h\eta_3\left(\eta_1+2\right)}{2\cos\theta\left(\eta_1-\sin\theta\right)};\ G_h = \frac{E_h}{2\left(1+\nu_h\right)};\ \ \eta_1 = \frac{d}{l};\ \ \eta_3 = \frac{t}{l}\end{aligned} \tag{4}$$

where E_{1c} and E_{2c} indicate the equivalent Young modulus, G_{12c}, G_{13c} and G_{23c} are the equivalent shear modulus; ρ_c and ν_{12c}, ν_{21c} are the equivalent mass density and Poisson's ratio of the core, respectively; E_h, ρ_h and ν_h describe the Young's modulus, mass density, and Poisson's ratio of the honeycomb material, respectively.

Following the refined plate theory, the displacement fields throughout the honeycomb sandwich plate are given by

$$\hat{\mathbf{u}} = \mathbf{u}_1 + z\mathbf{u}_2 + f\left(z\right)\mathbf{u}_3 \tag{5}$$

where

$$\widehat{\mathbf{u}}=\begin{Bmatrix}\widehat{u}\\ \widehat{v}\\ \widehat{w}\end{Bmatrix};\mathbf{u}_1=\begin{Bmatrix}u\\ v\\ w_b+w_s\end{Bmatrix};\mathbf{u}_2=\begin{Bmatrix}-w_{b,x}\\ -w_{b,y}\\ 0\end{Bmatrix};\mathbf{u}_3=\begin{Bmatrix}w_{s,x}\\ w_{s,y}\\ 0\end{Bmatrix} \tag{6}$$

in which $f(z)=-4z^3/3h^2$; u, and v are the displacements of the middle plane; w_b and w_s are the transverse displacement; the differential operator is denoted by symbol ",".

The strain tensor is expressed as follows

$$\boldsymbol{\varepsilon}=\begin{Bmatrix}\boldsymbol{\varepsilon}_b\\ \boldsymbol{\gamma}_s\end{Bmatrix}=\begin{Bmatrix}\boldsymbol{\varepsilon}_{b1}+z\boldsymbol{\varepsilon}_{b2}+f(z)\boldsymbol{\varepsilon}_{b3}\\ \left(1+f'(z)\right)\boldsymbol{\varepsilon}_s\end{Bmatrix} \tag{7}$$

in which

$$\boldsymbol{\varepsilon}_b=\begin{Bmatrix}\varepsilon_x\\ \varepsilon_y\\ \gamma_{xy}\end{Bmatrix};\boldsymbol{\varepsilon}_{b1}=\begin{Bmatrix}u_{,x}\\ v_{,y}\\ v_{,x}+u_{,y}\end{Bmatrix};\boldsymbol{\varepsilon}_{b2}=-\begin{Bmatrix}w_{b,xx}\\ w_{b,yy}\\ 2w_{b,xy}\end{Bmatrix};\boldsymbol{\varepsilon}_{b3}=\begin{Bmatrix}w_{s,xx}\\ w_{s,yy}\\ 2w_{s,xy}\end{Bmatrix};\boldsymbol{\gamma}_s=\begin{Bmatrix}\gamma_{xz}\\ \gamma_{yz}\end{Bmatrix};\boldsymbol{\varepsilon}_s=\begin{Bmatrix}w_{s,x}\\ w_{s,y}\end{Bmatrix} \tag{8}$$

The stress-strain relationship is expressed as follows

$$\begin{cases}\boldsymbol{\sigma}_b^{c,f}=\mathbf{C}_b^{c,f}\boldsymbol{\varepsilon}_b\\ \boldsymbol{\sigma}_s^{c,f}=\mathbf{C}_s^{c,f}\boldsymbol{\gamma}_s\end{cases} \tag{9}$$

where

$$\boldsymbol{\sigma}_b^{c,f}=\begin{Bmatrix}\sigma_x^{c,f}\\ \sigma_y^{c,f}\\ \tau_{xy}^{c,f}\end{Bmatrix}^T;\boldsymbol{\sigma}_s^{c,f}=\begin{Bmatrix}\tau_{xz}^{c,f}\\ \tau_{yz}^{c,f}\end{Bmatrix}^T;\mathbf{C}_{ub}^{c,f}=\begin{bmatrix}c_{11}^{c,f}&c_{12}^{c,f}&0\\ c_{12}^{c,f}&c_{22}^{c,f}&0\\ 0&0&c_{66}^{c,f}\end{bmatrix};\mathbf{C}_{us}^{c,f}=\begin{bmatrix}c_{55}^{c,f}&0\\ 0&c_{44}^{c,f}\end{bmatrix} \tag{10}$$

where c_{ij} represent the elastic coefficient; the symbols "c" and "f" indicate the core and face sheet, respectively. The elastic coefficients are defined as follows

$$\begin{gathered}c_{11}^c=\frac{E_{1c}}{1-\nu_{12c}\nu_{21c}};c_{12}^c=c_{21}^c=\frac{\nu_{12c}E_{2c}}{1-\nu_{12c}\nu_{21c}};c_{22}^c=\frac{E_{2c}}{1-\nu_{12c}\nu_{21c}};c_{44}^c=G_{23c};c_{55}^c=G_{13c};c_{66}^c=G_{12c}\\ c_{11}^f=c_{22}^f=\frac{E_f}{1-\nu_f^2};c_{12}^f=c_{21}^f=\frac{\nu_f E_f}{1-\nu_f^2};c_{44}^f=c_{55}^f=c_{66}^f=\frac{E_f}{2\left(1+\nu_f\right)}\end{gathered} \tag{11}$$

The Hamilton principle for static analysis is expressed as follows

$$\int_0^t\left(\delta U-\delta W\right)\mathrm{d}t=0 \tag{12}$$

in which U and W indicate the strain energy and work performed by an external load, respectively.

The virtual strain energy is presented as follows

$$\delta U=\int_{V_{top}}\left(\delta\boldsymbol{\varepsilon}_b^T\boldsymbol{\sigma}_b^f+\delta\boldsymbol{\varepsilon}_s^T\boldsymbol{\sigma}_s^f\right)\mathrm{d}V+\int_{V_{bottom}}\left(\delta\boldsymbol{\varepsilon}_b^T\boldsymbol{\sigma}_b^f+\delta\boldsymbol{\varepsilon}_s^T\boldsymbol{\sigma}_s^f\right)\mathrm{d}V+\int_{V_{core}}\left(\delta\boldsymbol{\varepsilon}_b^T\boldsymbol{\sigma}_b^c+\delta\boldsymbol{\varepsilon}_s^T\boldsymbol{\sigma}_s^c\right)\mathrm{d}V \tag{13}$$

where V refer to the volume of the plate.

Inserting Eq. (9) into Eq. (13), the variation of strain energy is reformed as follows

$$\delta U = \int_\Omega \delta \bar{\boldsymbol{\varepsilon}}_b^T \bar{\mathbf{D}}_b \bar{\boldsymbol{\varepsilon}}_b \mathrm{d}\Omega + \int_\Omega \delta \boldsymbol{\varepsilon}_s^T \bar{\mathbf{D}}_s \boldsymbol{\varepsilon}_s \mathrm{d}\Omega \tag{14}$$

with

$$\bar{\boldsymbol{\varepsilon}}_b = \begin{Bmatrix} \boldsymbol{\varepsilon}_{b1} \\ \boldsymbol{\varepsilon}_{b2} \\ \boldsymbol{\varepsilon}_{b3} \end{Bmatrix}; \quad \bar{\mathbf{D}}_b = \begin{bmatrix} \mathbf{A} & \mathbf{B} & \mathbf{E} \\ \mathbf{B} & \mathbf{D} & \mathbf{F} \\ \mathbf{E} & \mathbf{F} & \mathbf{H} \end{bmatrix}$$

$$\begin{aligned} (\mathbf{A},\mathbf{B},\mathbf{D},\mathbf{E},\mathbf{F},\mathbf{H}) &= \int_{-h/2}^{-h_c/2} \mathbf{C}_b^f \left(1, z, z^2, f, z\,f, f^2\right) \mathrm{d}z + \int_{-h_c/2}^{h_c/2} \mathbf{C}_b^c \left(1, z, z^2, f, z\,f, f^2\right) \mathrm{d}z + \\ &+ \int_{h_c/2}^{h/2} \mathbf{C}_b^f \left(1, z, z^2, f, z\,f, f^2\right) \mathrm{d}z \end{aligned} \tag{15}$$

$$\bar{\mathbf{D}}_s = \int_{-h/2}^{-h_c/2} (1+f') \mathbf{C}_s^f \mathrm{d}z + \int_{-h_c/2}^{h_c/2} (1+f') \mathbf{C}_s^c \mathrm{d}z + \int_{h_c/2}^{h/2} (1+f') \mathbf{C}_s^f \mathrm{d}z$$

Besides, the virtual work done by an external load is presented as follow

$$\delta W = \int_\Omega q_0 \delta \hat{w} \mathrm{d}\Omega \tag{16}$$

where q_0 represent the external transverse distributed load.

By replacing Eqs. (14) and (16) into Eq. (12), the governing equation of the honeycomb sandwich plate is rewritten as follows

$$\int_\Omega \delta \bar{\boldsymbol{\varepsilon}}_b^T \bar{\mathbf{D}}_b \bar{\boldsymbol{\varepsilon}}_b \mathrm{d}\Omega + \int_\Omega \delta \boldsymbol{\varepsilon}_s^T \bar{\mathbf{D}}_s \boldsymbol{\varepsilon}_s \mathrm{d}\Omega - \int_\Omega q_0 \delta \hat{w} \mathrm{d}\Omega = 0 \tag{17}$$

2.2. The isogeometric approximation

The displacement vector **u** is interpolated through NURBS basis functions [11] in the following manner

$$\mathbf{u}(x,y) = \sum_{e=1}^{m \times n} \mathbf{N}_e (x,y) \boldsymbol{\eta}_e \tag{18}$$

where

$$\mathbf{N}_e (x,y) = \begin{bmatrix} 1 & 0 & 0 & 0 \\ 0 & 1 & 0 & 0 \\ 0 & 0 & 1 & 0 \\ 0 & 0 & 0 & 1 \end{bmatrix} N_e (x,y); \quad \boldsymbol{\eta}_e = \begin{Bmatrix} u_e \\ v_e \\ w_{be} \\ w_{se} \end{Bmatrix} \tag{19}$$

where the NURBs basic functions are indicated by $N_e(x,y)$. Compared with conventional FEM shape functions, NURBS basis functions preserve the exact geometry of the plate and provide higher-order continuity across elements. This capability is particularly advantageous for sandwich plates with curved boundaries or slender geometries, where FEM may require complex meshing and still introduce geometric approximation errors.

After substituting Eq. (18) into Eq. (7), the linear strain is reformulated as follows

$$\bar{\boldsymbol{\varepsilon}}_b = \sum_{e=1}^{m \times n} \begin{Bmatrix} \mathbf{B}_{b1e} \\ \mathbf{B}_{b2e} \\ \mathbf{B}_{b3e} \end{Bmatrix} \boldsymbol{\eta}_e = \sum_{e=1}^{m \times n} \bar{\mathbf{B}}_{be} \boldsymbol{\eta}_e ; \boldsymbol{\varepsilon}_s = \sum_{e=1}^{m \times n} \bar{\mathbf{B}}_{se} \boldsymbol{\eta}_e \tag{20}$$

in which

$$\mathbf{B}_{b1e}=\begin{bmatrix} N_{e,x} & 0 & 0 & 0 \\ 0 & N_{e,y} & 0 & 0 \\ N_{e,y} & N_{e,x} & 0 & 0 \end{bmatrix};\mathbf{B}_{b2e}=-\begin{bmatrix} 0 & 0 & N_{e,xx} & 0 \\ 0 & 0 & N_{e,yy} & 0 \\ 0 & 0 & 2N_{e,xy} & 0 \end{bmatrix};\mathbf{B}_{b3e}=\begin{bmatrix} 0 & 0 & 0 & N_{e,xx} \\ 0 & 0 & 0 & N_{e,yy} \\ 0 & 0 & 0 & 2N_{e,xy} \end{bmatrix}$$
$$\bar{\mathbf{B}}_{se}=\begin{bmatrix} 0 & 0 & 0 & N_{e,x} \\ 0 & 0 & 0 & N_{e,y} \end{bmatrix} \tag{21}$$

Substituting Eq. (21) into Eq. (17), the governing equations for the static bending of the auxetic honeycomb sandwich plate are reformulated as follows

$$\mathbf{K}\boldsymbol{\eta}=\mathbf{F} \tag{22}$$

where

$$\mathbf{K}=\int_\Omega \bar{\mathbf{B}}_b^T\bar{\mathbf{D}}_b\bar{\mathbf{B}}_b\mathrm{d}\Omega+\int_\Omega \bar{\mathbf{B}}_s^T\bar{\mathbf{D}}_s\bar{\mathbf{B}}_s\mathrm{d}\Omega;\mathbf{F}=\int_\Omega q_0\mathbf{B}_F\mathrm{d}\Omega;\ \mathbf{B}_F=\begin{Bmatrix}0 & 0 & N_e & N_e\end{Bmatrix} \tag{23}$$

where **K** and **F** represent the stiffness matrix and force vector, respectively

3. Numerical results

This section focuses on analyzing the sandwich rectangular plates with GNPs facelayers and auxetic honeycomb core, and subjected to a range of boundary conditions (BCs). The prescribed Dirichlet boundary conditions applied to the rectangular plate are specified as follows.

- Simply supported (SSSS): $\left(u,w_b,w_s\right)\big|_{xy=0,b}=0;\left(v,w_b,w_s\right)\big|_{x=0,a}=0$
- Fully clamped (CCCC): $\left(u,v,w_b,w_{b,n},w_{s,n}\right)\big|_{x=0,a;y=0,b}=0$
- Simply supported at x=0, a and clamped at y=0, b (SCSC): $\begin{cases}\left(v_0,w_b,w_s\right)\big|_{x=0,a}=0\\ \left(u_0,v_0,w_b,w_{b,n},w_s,w_{s,n}\right)\big|_{y=0,b}=0\end{cases}$

The mechanical properties of the honeycomb core and GNPs face sheet layers are defined as follows [19]: $E_m=E_h=70\,\mathrm{GPa}$, $\nu_m=\nu_h=0.3$, $\rho_m=\rho_h=2707\,\mathrm{kg/m^3}$, $\eta_3=0.0138571$, $E_G=1010\,\mathrm{GPa}$, $\nu_G=0.186$, $\rho_G=1062.5\,\mathrm{kg/m^3}$, $l_G=2.5\,\mu\mathrm{m}$, $w_G=1.5\,\mu\mathrm{m}$, $t_G=1.5\,\mathrm{nm}$.

Firstly, the static bending of the plate made of aluminum reinforced by GNPs, with the material parameters given in [20], was examined to verify the accuracy and reliability of the proposed model. The percentage deflection ratio w_C/w_M for GNPs/epoxy nanocomposite plates with uniform GNPs distribution patterns and under uniform transverse distributed load q_0 is plotted in Figure 2, where w_C and w_M represent the central deflections of the plates with and without GNPs reinforcement, respectively. The percentage deflection ratio is compared with the values provided by Song et al. [20] using FSDT and the Navier method. As seen in Figure 2, the present numerical results match the reference solution very well. The above example clearly demonstrates that the proposed method is both accurate and effective in predicting the static behavior of the sandwich plate with GNPs facesheets and honeycomb core.

Next, new insights into the static analysis of sandwich plates with GNPs facesheets under uniform transverse distributed load are presented. A normalized central deflection is obtained by dividing by: $\tilde{w}=\dfrac{wE_mh^3}{12q_0L^4\left(1-\nu_m^2\right)}$. The effect of the cell inclined angle (θ) and core-to-face thickness ratio (h_c/h_f) on the normalized central deflection of sandwich plates is listed in Table 1. Table 1 shows that, as the

parameter θ increases, a reduction in the normalized central deflection is observed. This trend results from the improved load transfer efficiency of the honeycomb structure, as steeper ribs provide enhanced resistance to bending. Moreover, the table demonstrates that the deflection values are significantly influenced by the BCs. Among the three BCs, the CCCC sandwich plate produces the lowest deflections due to its fully clamped nature, which effectively restricts both translations and rotations at all edges. The SSSS and SCSC conditions show higher deflections, but still exhibit a similar decreasing trend with increasing angle, confirming that well-constrained edges enhance the structural stiffness and reduce overall deflection. Furthermore, the auxetic effect of the honeycomb core also contributes to reducing deflection, as the negative Poisson's ratio mechanism enhances lateral expansion under load, improving energy absorption and overall stiffness.

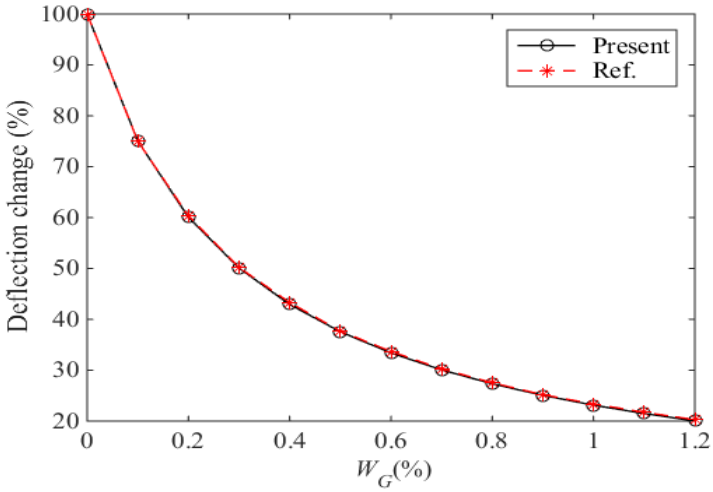

Figure 2. *The percentage deflection ratio w_C/w_M for GNPs/epoxy nanocomposite with various GNPs weight fractions (a/h = 10).*

Table 1. *The impact of the cell inclined and core-to-face thickness ratio on the normalized central deflection of the honeycomb square sandwich plate (a/h = 10, η_1=1.5, W_G = 1%).*

BCs	hc/h_f	θ				
		15^0	30^0	45^0	60^0	75^0
SSSS	4	0.6136	0.6103	0.6045	0.5933	0.5662
	6	0.8724	0.8593	0.8593	0.7997	0.7239
	8	1.1694	1.1358	1.0840	1.0018	0.8643
	10	1.4750	1.4108	1.3178	1.1831	0.9881
CCCC	4	0.3037	0.3006	0.2952	0.2848	0.2599
	6	0.4870	0.4747	0.4546	0.4195	0.3494
	8	0.7043	0.6730	0.6249	0.5486	0.4210
	10	0.9292	0.8695	0.7829	0.6575	0.4760
SCSC	4	0.3790	0.3756	0.3698	0.3586	0.3319
	6	0.5829	0.5699	0.5483	0.5106	0.4363
	8	0.8226	0.7895	0.7380	0.6565	0.5225
	10	1.0707	1.0073	0.9148	0.7816	0.5922

Table 2 investigates the combined influence of the geometric factor η_1 and the width-to-length ratio (b/a) on the normalized central deflection under three different boundary conditions: SSSS, CCCC, and SCSC. The results clearly show that for all boundary conditions, the normalized central deflection increases monotonically with both increasing η_1 and increasing width-to-length ratio. Increasing the geometric parameter η_1 leads to a notable rise in central deflection, which is associated with the reduced stiffness of the core due to more flexible cell geometry. Similarly, a higher width-to-length ratio results in greater deflection due to the larger unsupported span in the transverse direction. Figure 3 shows how the GNPs weight fraction (W_G) and length-to-thickness ratio (a/h) influence on the normalized central deflection of the sandwich square plate. The data in Figure 3 indicate that the normalized central deflection reduces as the parameter W_G increases, indicating the stiffening effect of GNPs reinforcement. An increase in the a/h ratio leads to a slight rise in deflection, which then stabilizes at greater values. These results highlight the combined influence of GNPs content and BCs on improving the flexural stiffness of sandwich plates.

Table 2. *The effect of the factor η_1 and width-to-length ratio on the normalized central deflection (a/h = 10, $h_c/h_f = 8, \theta = 15^0, W_G$ = 1%).*

BCs	b/a	η_1						
		0.8	1.0	1.2	1.4	1.6	1.8	2.0
SSSS	1	1.0658	1.1108	1.1403	1.1611	1.1765	1.1883	1.1977
	1.5	1.8560	1.9010	1.9284	1.9467	1.9597	1.9693	1.9766
	2	2.3605	2.3973	2.4184	2.4317	2.4407	2.4471	2.4518
	2.5	2.6444	2.6734	2.6889	2.6982	2.7042	2.7082	2.7110
	3	2.7972	2.8202	2.8320	2.8386	2.8426	2.8451	2.8467
CCCC	1	0.6088	0.6502	0.6775	0.6967	0.7109	0.7218	0.7304
	1.5	0.9650	1.0066	1.0321	1.0490	1.0610	1.0699	1.0767
	2	1.1423	1.1765	1.1961	1.2085	1.2168	1.2228	1.2272
	2.5	1.2230	1.2499	1.2645	1.2732	1.2788	1.2826	1.2853
	3	1.2606	1.2822	1.2933	1.3034	1.3034	1.3059	1.3075
SCSC	1	0.7258	0.7680	0.7956	0.8150	0.8293	0.8402	0.8489
	1.5	1.0225	1.0635	1.0885	1.1050	1.1167	1.1253	1.1319
	2	1.1643	1.1975	1.2164	1.2282	1.2362	1.2419	1.2460
	2.5	1.2309	1.2569	1.2708	1.2790	1.2843	1.2879	1.2903
	3	1.2635	1.2843	1.2948	1.3007	1.3043	1.3065	1.3080

To show the advantage of the proposed model, the bending analysis of the circular auxetic sandwich plate, under the fully clamped (CC) and fully simply supported (SS) boundaries, is studied. Table 3 presents the normalized central deflection $\tilde{w}_c = \dfrac{wE_m h^3}{12q_0 R^4\left(1-\nu_m^2\right)}$ of the sandwich plate under different cell inclinations and core-to-face thickness ratios. The results show that deflection of the circular auxetic sandwich plate decreases as the cell inclination increases, indicating improved load transfer efficiency of steeper cell walls. Moreover, increasing the core-to-face thickness ratio leads to higher deflections due to the reduced bending stiffness.

Table 3. *The normalized central deflection of the honeycomb circular sandwich plate under the impact of the cell inclined and core-to-face thickness ratio (R/h=10, η_1=1.5, W_G = 1%).*

BCs	hc/h_f	θ				
		15^0	30^0	45^0	60^0	75^0
SS	4	7.4141	7.4046	7.3852	7.3460	7.2487
	6	9.4483	9.4072	9.3345	9.2046	8.9400
	8	11.6518	11.5434	11.3689	11.0906	10.6155
	10	13.9025	13.6923	13.3790	12.9259	12.2509
CC	4	2.2533	2.2425	2.2236	2.1874	2.1006
	6	3.1511	3.1084	3.0381	2.9164	2.6757
	8	4.1759	4.0665	3.8983	3.6357	3.2010
	10	5.2306	5.0209	4.7189	4.2898	3.6734

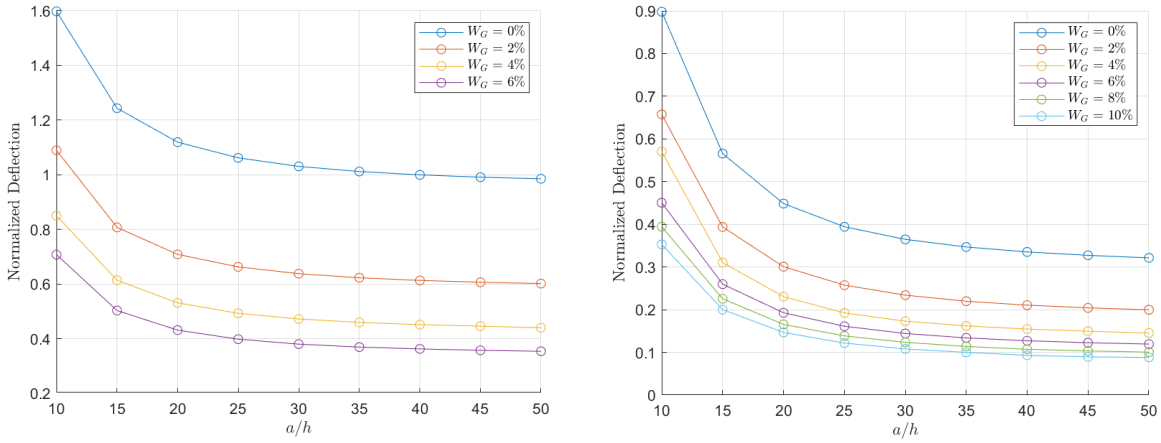

a) SSSS b) CCCC

Figure 3. *The impact of the parameters a/h and W_G on the normalized central deflection of the square auxetic sandwich plate ($h_c / h_f = 10$, $\theta = 15^0$, $\eta_1 = 0.8$)*

4. Conclusions

This paper has investigated the static response of auxetic honeycomb sandwich plates with graphene nanoplatelet (GNP)-reinforced facesheets using an RPT in conjunction with the IGA framework. The equivalent material properties of the nanocomposite face sheets were estimated through a modified Halpin–Tsai model. Numerical simulations were conducted to evaluate the influence of the cell inclination angle, geometric coefficient η_1, width-to-length ratio, and boundary conditions on the normalized central deflection of the sandwich structure. The results revealed that increasing the cell angle leads to a significant reduction in central deflection, attributed to the stiffening of the honeycomb geometry. In contrast, higher values of the geometric coefficient η_1 or the width-to-length ratio cause an increase in deflection due to reduced core stiffness. Among the BCs, CCCC configurations exhibited the greatest resistance to deformation, while SCSC showed comparatively larger deflections. Overall, the combination of auxetic honeycomb cores and GNP-reinforced face sheets provides a promising design for enhancing the mechanical performance of lightweight sandwich structures. The proposed IGA-based approach demonstrated high accuracy and efficiency in capturing the complex behavior of the system, offering a reliable tool for advanced composite design.

Conflict of Interest

The authors declare no conflict of interest.

Acknowledgment

This work belongs to the project grant No: SV2025-245 funded by Ho chi Minh city university of Technology and Education, Vietnam.

REFERENCES

[1] J. Liu, Y. Cheng, R. Li, and F. Au, "A semi-analytical method for bending, buckling, and free vibration analyses of sandwich panels with square-honeycomb cores," *International Journal of Structural Stabilityand Dynamics,* vol. 10, no. 01, pp. 127-151, 2010.
[2] P. R. Jeyakrishnan, K. K. S. K. Chockalingam, and R. Narayanasamy, "Studies on buckling behavior of honeycomb sandwich panel," *The International Journal of Advanced Manufacturing Technology,* vol. 65, no. 5, pp. 803-815, 2013.
[3] P. T. Thang, "Buckling analysis of graphene nanoplatelets/polymer composite sandwich cylindrical shells with auxetic honeycomb core under external pressure," *Mechanics Based Design of Structures and Machines,* vol. 53, no. 10, pp. 6722-6748, 2025.
[4] F. Shirdelan, M. Mohammadimehr, and F. Bargozini, "Control and vibration analyses of a sandwich doubly curved micro-composite shell with honeycomb, truss, and corrugated cores based on the fourth-order shear deformation theory," *Applied Mathematics and Mechanics,* vol. 45, no. 10, pp. 1773-1790, 2024.
[5] S. J. Singh, V. Kumar, D. Mehta, V. Kumar, and S. P. Harsha, "Vibration and Buckling Characteristics of Sandwich FGM Plate with Conventional and Auxetic Honeycomb Core," *International Journal of Structural Stability and Dynamics,* vol. 25, no. 08, p. 2550081, 2024.
[6] W. Yuan, H. Liao, R. Gao, and Y. Chen, "Buckling Stability and Vibration Characteristics of Functionally Graded Graphene Platelet-Reinforced Composites Multi-Arc Concave Honeycomb Sandwich Panels Under Thermal Loading," *International Journal of Structural Stability and Dynamics,* vol. 24, no. 18, p. 2450200, 2023.
[7] F. Ebrahimi, D. Hashemabadi, M. Habibi, and H. Safarpour, "Thermal buckling and forced vibration characteristics of a porous GNP reinforced nanocomposite cylindrical shell," *Microsystem Technologies,* vol. 26, no. 2, pp. 461-473, 2020.
[8] A. S. Khalaf and H. M. Hasan, "Nonlinear forced vibration of functionally graded hybrid three-phase nanocomposite toroidal shell segments reinforced by carbon nanotubes (CNTs) and graphene nanoplatelets (GPLs)," *Thin-Walled Structures,* vol. 199, p. 111876, 2024.
[9] T. Zhao, M. J. Bayat, A. kalhori, and K. Asemi, "Free vibration analysis of functionally graded multilayer hybrid composite cylindrical shell panel reinforced by GPLs and CNTs surrounded by Winkler elastic foundation," *Engineering Structures,* vol. 308, p. 117975, 2024.
[10] J. Li, F. Tang, and M. Habibi, "Bi-directional thermal buckling and resonance frequency characteristics of a GNP-reinforced composite nanostructure," *Engineering with Computers,* vol. 38, no. 2, pp. 1559-1580, 2022.
[11] T. J. Hughes, J. A. Cottrell, and Y. Bazilevs, "Isogeometric analysis: CAD, finite elements, NURBS, exact geometry and mesh refinement," *Computer methods in applied mechanics and engineering,* vol. 194, no. 39-41, pp. 4135-4195, 2005.
[12] T. H. N. Thi, V. K. Tran, and Q. H. Pham, "An isogeometric approach for nonlocal bending and free oscillation of magneto-electro-elastic functionally graded nanobeam with elastic constraints," *Frontiers of Structural and Civil Engineering,* vol. 18, no. 9, pp. 1401-1423, 2024.
[13] P. Phung-Van, C. H. Thai, H. Nguyen-Xuan, and M. Abdel-Wahab, "An isogeometric approach of static and free vibration analyses for porous FG nanoplates," *European Journal of Mechanics - A/Solids,* vol. 78, p. 103851, 2019.
[14] M. Lezgy-Nazargah, P. Vidal, and O. Polit, "NURBS-based isogeometric analysis of laminated composite beams using refined sinus model," *European Journal of Mechanics-A/Solids,* vol. 53, pp. 34-47, 2015.
[15] P. Shi, C. Dong, H. Shou, and B. Li, "Bending, vibration and buckling isogeometric analysis of functionally graded porous microplates based on the TSDT incorporating size and surface effects," *Thin-Walled Structures,* vol. 191, p. 111027, 2023.
[16] J. H. Affdl and J. Kardos, "The Halpin-Tsai equations: a review," *Polymer Engineering & Science,* vol. 16, no. 5, pp. 344-352, 1976.
[17] R. G. D. Villoria and A. Miravete, "Mechanical model to evaluate the effect of the dispersion in nanocomposites," *Acta Materialia,* vol. 55, no. 9, pp. 3025-3031, 2007.
[18] X. Zhu, J. Zhang, W. Zhang, and J. Chen, "Vibration frequencies and energies of an auxetic honeycomb sandwich plate," *Mechanics of Advanced Materials and Structures,* vol. 26, no. 23, pp. 1951-1957, 2019.
[19] N. V. Nguyen, H. Nguyen-Xuan, T. N. Nguyen, J. Kang, and J. Lee, "A comprehensive analysis of auxetic honeycomb sandwich plates with graphene nanoplatelets reinforcement," *Composite Structures,* vol. 259, p. 113213, 2021.
[20] M. Song, J. Yang, and S. Kitipornchai, "Bending and buckling analyses of functionally graded polymer composite plates reinforced with graphene nanoplatelets," *Composites Part B: Engineering,* vol. 134, pp. 106-113, 2018.

Minh Anh Hoang was born in Vietnam in 2005. She is currently an undergraduate student majoring in construction management at Ho Chi Minh City University of Technology and Education, Ho Chi Minh City, Vietnam.
Email address: 22155005@student.hcmute.edu.vn. ORCID: https://orcid.org/0009-0002-4768-1387

Tri Dung Nguyen was born in Vietnam in 2002. He is currently an undergraduate student majoring in Civil Engineering at Ho Chi Minh City University of Technology and Education, Ho Chi Minh City, Vietnam.
Email address: 20149124@student.hcmute.edu.vn. ORCID: https://orcid.org/0009-0004-3500-6282

Tan Hung Pham was born in Vietnam in 1981. He has a Ph.D. degree in Mechanics. Now, he is a lecturer at the Faculty of Civil Engineering at Ho Chi Minh City University of Technology and Education, Ho Chi Minh City, Vietnam. His research interests are the computational mechanics.
Email address: hungpht@hcmute.edu.vn. ORCID: https://orcid.org/0000-0001-6105-9311